JRC Technical Notes

IMAGE-2006 Mosaic: SPOT-HRVIR and IRS-LISSIII Cloud Detection

v.1.0

Pierre Soille

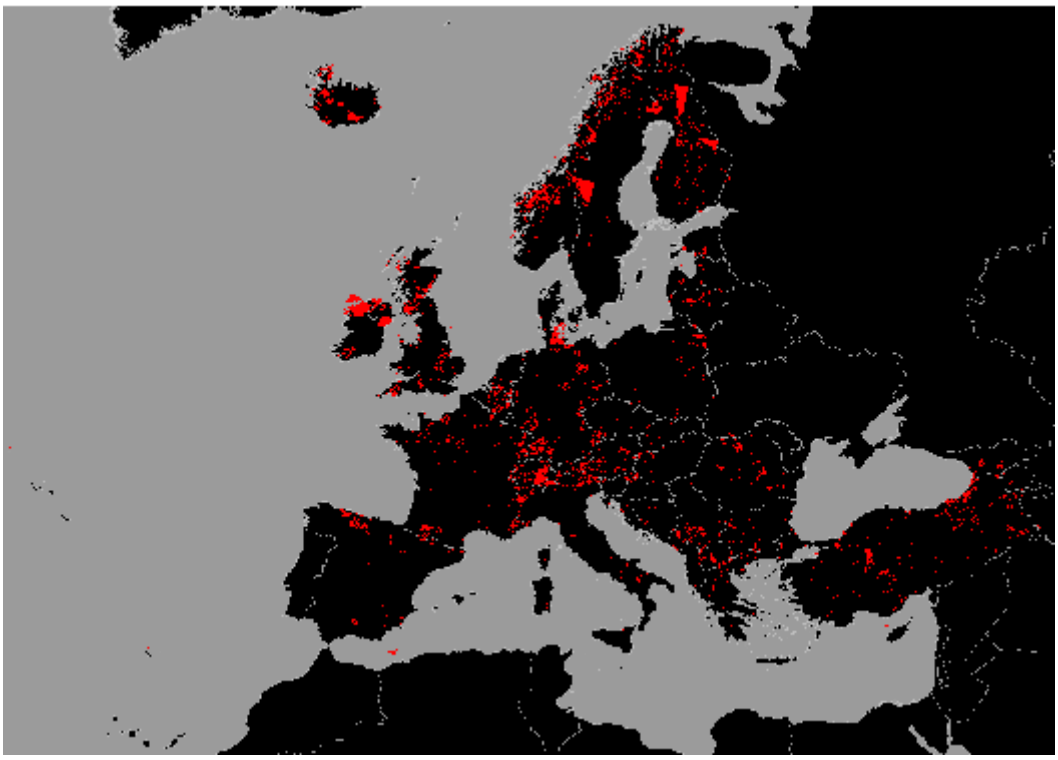

EUR 23636 EN

JRC EUROPEAN COMMISSION

ies Institute for Environment and Sustainability

The mission of the Institute for Environment and Sustainability is to provide scientific-technical support to the European Union's Policies for the protection and sustainable development of the European and global environment.

European Commission
Joint Research Centre
Institute for Environment and Sustainability
Spatial Data Infrastructures Unit

Contact information
Address: via E. Fermi 2749, I-21027 Ispra (Italy)
E-mail: Pierre.Soille@jrc.ec.europa.eu
Tel.: int+39-0332 785 068
Fax: int+39-0332 786 325

http://ies.jrc.ec.europa.eu/
http://www.jrc.ec.europa.eu/

JRC 48716

EUR 23636 EN
ISBN 978-92-79-20955-0
ISSN 1831-9424
doi:10.2788/49355

Luxembourg: Publications Office of the European Union, 2011

IMAGE-2006 Mosaic: Cloud Detection on SPOT-4 HRVIR, SPOT-5 HRG, and IRS-LISS III —v.1.0—

Pierre Soille
COSIN Action
IES-Spatial Data Infrastructures Unit

November 26, 2008

Abstract

This report details the methodology adopted for detecting clouds from the IMAGE-2006 SPOT-4 HRVIR, SPOT-5 HRG, and IRS-LISS III imagery in view of creating mosaics. This detection is necessary for minimising cloud cover. Indeed, when clouds appear in a region where two or more images overlap, an image with no clouds in this region must be selected to cover this region. The availability of cloud masks enables an automatic selection during mosaicing. The proposed methodology is based on a modified cloud detection algorithm originally developed for Landsat sensors. The modifications address the lack of a thermal channel for the IMAGE-2006 imagery. Spatial context is also exploited in a second stage thanks to a series of morphological transformations. Overall, the produced cloud masks are satisfactory for automatically minimising cloud cover during mosaicing.

Contents

1 Introduction

Because clouds mask the ground in the optical domain, cloud free images should be selected whenever possible. However, this is difficult if not impossible to achieve in some regions. For these regions, cloud free coverage is only possible thanks to multiple acquisitions. This explains why some areas are covered several times in the IMAGE-2006 coverages. The amount of cloud cover within the mosaic will be minimised because the developed morphological image compositing method takes cloud masks into account. Indeed, during mosaicing, cloud free image pieces are automatically selected. Hence, the automatic mosaicing procedure requires a cloud mask to be available for each input image.

This report details the methodology developed for automatically generating cloud masks. This methodology is based on the analysis of Top of Atmosphere (TOA) reflectance values rather than the input digital numbers. The conversion from input digital numbers to TOA reflectance values is based on Look-Up-Tables (LUTs) described in Sec. 2. The cloud detection method itself is detailed in Sec. 3 with its two main steps: unsupervised classification exploiting spectral attributes followed by a series of morphological transformations exploiting spatial attributes. Before concluding, results are presented and discussed in Sec. 4.

2 Digital numbers to TOA reflectance LUTs

The values of the pixels of any given input image are usually referred to as digital numbers (DNs). They can be converted to radiance values by applying a linear transformation. However, because the parameters (i.e., gain and offset) of this linear transformation vary from one image to another, the input DNs originating from two different images are not necessarily comparable. Therefore, the application of fixed threshold levels to DNs is not robust. Even after conversion to radiance values, fixed threshold levels should not be applied because the radiance values depend themselves on the date and time of acquisition (varying Earth-Sun distance and sun elevation angle). This dependence can be suppressed (or at least mitigated) by converting the radiance values into reflectance values (i.e., proportion of the incident energy that is reflected). Fixed threshold levels can be applied to reflectance values.

Ideally, reflectance should be measured at the ground level. However, measurements are performed by the satellite at the TOA level. The conversion from TOA to ground reflectance values requires ancillary data about the atmospheric condition at the time of acquisition and/or user-interaction to select the pixels that are deemed to be the clearest. This is for instance the case of the haze optimised transform described in [18]. Given the available data and resources for the IMAGE-2006 Mosaic project, it was decided to use TOA reflectance values as a proxy for the desired ground reflectance values.

The TOA reflectance values are calculated using the gain, offset, acquisition date, sun elevation angle ϕ, and solar irradiance values retrieved from the header file of the corresponding band (see details in [13]). The required formulæ can be found for example in [11] and are summarised hereafter. Denoting by x_i a digital number in the ith band, the corresponding TOA radiance L_i is calculated using the gain g_i and offset o_i values retrieved from the header file of the ith

Table 1: Julian Day (J.D.) to Earth-Sun distance d in astronomical units. [Source: USGS, see http://eo1.usgs.gov/faq.php?id=25].

J.D.	d	J.D.	d	J.D.	d	J.D.	d	J.D.	d
1	.9832	74	0.9945	152	1.0140	227	1.0128	305	.9925
15	.9836	91	0.9993	166	1.0158	242	1.0092	319	.9892
32	.9853	106	1.0033	182	1.0167	258	1.0057	335	.9860
46	.9878	121	1.0076	196	1.0165	274	1.0011	349	.9843
60	.9909	135	1.0109	213	1.0149	288	0.9972	365	.9833

band:

$$L_i = (x_i - o_i)/g_i,$$

in $\mathrm{W}\times\mathrm{m}^{-2} \times \mathrm{sr}^{-1}\times\mu\mathrm{m}^{-1}$. The TOA reflectance ρ is then calculated by taking into account the sun zenith angle θ (complement of the sun elevation angle ϕ: $\theta = \pi/2 - \phi$) and the Earth-Sun distance d (in astronomical units) at the date of acquisition as well as the mean exoatmospheric solar irradiance E (in $\mathrm{W}\times\mathrm{m}^{-2}\times\mu\mathrm{m}^{-1}$) of band i:

$$\rho_i = \pi L_i d^2/(E_i \cos\theta).$$

The Earth-Sun distance can be interpolated from the values given in table 1. Alternatively, it can be calculated for any single Julian day[1] using astronomical algorithms described in [10]. The reflectance is a unitless quantity whose values range from 0 (no incident energy reflected) to 1 (all incident energy is reflected).

In practice, the conversion from DNs to TOA reflectance values is achieved thanks to a TIFF image containing a unique line of 256 pixels with float values between 0.0 and 1.0. It corresponds to a LUT mapping the DNs to the TOA reflectance values. For example, the TOA value of the digital number with value 0 is given by the value of the first pixel of this LUT. By doing so, the above formulæ need to be computed only once for each 256 possible DN value rather than for each pixel.

3 Methodology

The Automatic Cloud Cover Assesment (ACCA) put forward in [5] is a proven method for detecting clouds with Landsat imagery. ACCA is an unsupervised classifier for clouds that takes advantage of known properties of clouds, snow, bright soil, vegetation, and water. A detailed analysis of the reliability of this algorithm as well as its failure modes (mainly semi-transparent clouds such as of cirrus and cloud edges) is reported in [6]. Beyond the spectral bands available for SPOT-4 HRVIR, SPOT-5 HRG, and IRS-LISS III imagery, ACCA exploits the measured reflectance values in the blue, mid infrared in the range 2.08–2.35 µm, and thermal bands. Unfortunately, these latter 3 bands are not available for these sensors. To solve this problem, the proposed methodology

[1] Julian dates were calculated using the algorithm described in [3].

relies on a modified ACCA algorithm (Sec. 3.1) followed by a series of morphological transformations exploiting spatial attributes (Sec. 3.2). All stored data is summarised in Sec. 3.3.

3.1 First step: modified ACCA algorithm

For the purpose of IMAGE-2006 mosaicing, the automatic cloud cover assessment (ACCA) algorithm developed in [5, 6] for Landsat images was adapted to SPOT and IRS images. Given that only 4 of the 7 bands of Landsat TM imagery are available for SPOT0-4 HRVIR, SPOT-5 HRG, and IRS-LISS III imagery (see above), only ACCA filters 1–2 and 5–7 of the so-called 'pass one' [5] can be retained without any modification. The other filters have been replaced by ad hoc procedures. ACCA filter 3 (originally temperature threshold based on thermal band) was replaced by a threshold on the arithmetic difference between band 3 and band 2. ACCA Filter 4 (originally Landsat band 5/band 6 composite) was replaced by an intensity threshold on band 1. ACCA filter 8 has been discarded as well as ACCA 'pass two' processing because they require the availability of the thermal channel [5]. A brief description of each filter is given hereafter[2]:

- Filter 1: brightness threshold. All pixels in band 2 whose reflectance is below 0.08 are classified as non-cloud [5].
- Filter 2: normalised difference snow index (NDSI). This index is defined as follows [4]:

  $$\text{NDSI} = (\text{band } 1 - \text{band } 4)/(\text{band } 1 + \text{band } 4).$$

  All pixels whose NDSI exceeds 0.7 are classified as non-cloud [5].
- Filter 3: difference between band 3 and band 2. All pixels whose reflectance in band 3 is not at least 0.05 greater than in band 2 are classified as non-cloud.
- Filter 4: intensity threshold on band 1 only. All pixels whose band 1 reflectance is less than 0.1 are classified as non-cloud.
- Filter 5: band 3/band 2 ratio. All pixels whose ratio exceeds 2.0 are classified as non-cloud [5].
- Filter 6: band 3/band 1 ratio. All pixels whose ratio exceeds 2.0 are classified as non-cloud [5].
- Filter 7: band 3/band 4 ratio. All pixels whose ratio exceeds 1.0 are classified as non-cloud [5].

All potential cloud pixels in the image mask corresponding to the ith filter are set to 2^{i-1}, the non-cloud pixels being set to 0. This enables the combination of all 7 individual masks into a unique image by simply computing the bitwise union operation between all 7 individual masks. Therefore, in this resulting combined

[2]Due to the absence of the blue channel for SPOT-4 HRVIR, SPOT-5 HRG, and IRS-LISS III images, the band number indices given in this report need to be incremented by one when considering Landsat data.

image, the maximum value of a pixel equals 127 (all 7 filters returning potential cloud). Examples are displayed in the middle image column of Fig. 1 (the generation of the binary cloud masks displayed in the right column is detailed in the next section). The input images have been rendered by mapping the bands 4, 3, and 1 to the red, green, and blue channels (false colour composition).

3.2 Second step: spatial context

Unfortunately, due to the lack of a thermal band, those pixels of the `IM-ACCA` images that return potential clouds for all 7 filters (i.e., pixels with value 127 in `IM-ACCA`) lead to mainly true positive detection but contain many false negative errors. Therefore, these pixels are merely considered as markers indicating the presence of clouds with a high degree of confidence. These markers are then used as seeds for initiating a region growing process expanding the marker set until the full cloudy regions are reached. More precisely, the binary mask of clouds is generated by considering the morphological reconstruction by dilation [12] of the pixels with value 127 (i.e., potential clouds for all 7 filters) using as geodesic mask these pixels plus those with value 79 (all but filters 5 and 6 returning cloud), 95 (all but filter 6 returning cloud), and 111 (all but filter 5 returning cloud). The resulting mask is then cleaned by filling all its holes and then suppressing all connected components not containing at least one cloud block of 4×4 pixels. Note that, with the proposed methodology, clouds need to contain at least one pixel with value 127 in the ACCA image because otherwise the region growing process cannot be initiated.

Examples showing the input images, the images combining the output of all 7 individual filters, and the resulting binary cloud masks are given in Fig. 1.

3.3 Stored data

All relevant data related to cloud detection is stored in the ancillary directories `2006_COV1_ANC`, `2006_COV2_ANC`, and `2006_REF_ANC`:

- DN to TOA LUTs. For the reference coverage, their type and identifier fields are set to the following values: `IP-L10C` for band 1, `IP-L20C` for band 2, etc. For the individual coverages, the `0C` characters are replaced by the appropriate country code `XX`: `IP-L1XX`, etc.;
- ACCA outputs with bitwise coding of each filter: For the reference coverage, these results stored in the image file using `IM-ACCA` as type/identifier field (plus the country code for images originating from the individual coverages: `IM-ACCAXX`);
- binary cloud masks: The type and identifier field of the binary cloud masks is set to `IM-CLDS` in the case of the reference coverage. For the individual coverages, the `DS` letters are replaced by the two letter country code: `IM-CLXX`.

All this data occupies approximately 16 Gbytes on disk.

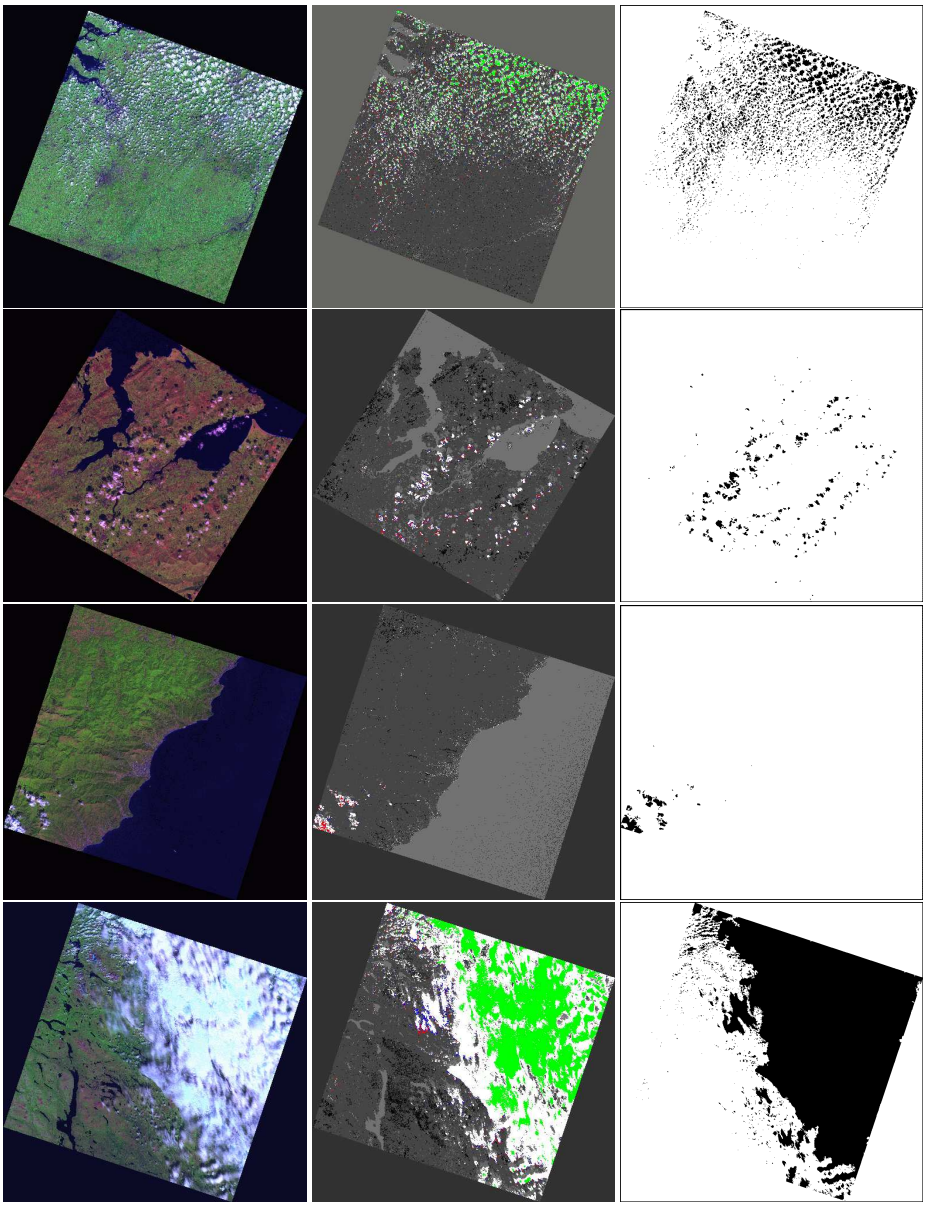

Figure 1: IMAGE-2006 cloud detection. Left column: input images. Middle column: output of modified ACCA filters coded on 7 bit planes with white for code 127 (all filters returning potential clouds), red for code 79 (all but filters 5 and 6 returning cloud), green for code 95 (all but filter 6 returning cloud), and blue for code 111 (all but filter 5 returning cloud). Right column: Resulting binary cloud masks. Input images (from top to bottom, all from coverage 1): `20060710-1051 IL3 BE 3955931097-CB`, `20060404-1149 SP4 IE 3225036819-CB`, `20060830-1035 SP5 IT 4179723343-DA`, and `20060715 IL3 NO 4469843797-AB`.

4 Results

The produced cloud masks are evaluated in Sec. 4.1. Success and failure modes of the proposed methodology are also reported and illustrated. Summary statistics are presented in Sec. 4.2.

4.1 Cloud masks

Overall, for the purpose of minimising cloud cover when mosaicing, the quality of the produced cloud masks is sufficient. A gallery of 27 examples of satisfactory cloud masks in a range of landscapes and latitudes is displayed in Fig. 2. Nevertheless, given the absence of a thermal band, it is not possible to avoid false positive and false negative errors when detecting clouds from SPOT-4 HRVIR/SPOT-5 HRG and IRS-LISS III images with the procedure described in Sec. 3. A gallery illustrating cases where the algorithm is failing to detect clouds or wrongly detecting non-cloud objects as clouds is displayed in Fig. 3. Most false positive errors are due to ice and snow fields detected as clouds. Fortunately, this type of error is not an issue in view of creating a mosaic because it is usually desirable to minimise snow/ice covered areas. For instance, a 30th of December scene with snow will be automatically discarded (see example in Fig. 6). A series of false negative errors may also occur. This is the case for some bare soil fields, roofs of large buildings, and a few beaches detected as clouds (see gallery). Furthermore, semi-transparent clouds and thin clouds over the sea are also missed. This latter limitation is also reported for the original ACCA procedure on Landsat imagery [6]. Note that the detection of clouds over the sea is not critical for mosaicing purposes since, although undesirable, they are not masking out the terrain.

All images of Figs. 2–3 were extracted from a mosaic image combining all available imagery of the first coverage by performing the point-wise maximum operation between all images. It follow that all clouds are revealed in this mosaic because clouds are reflecting more than land cover classes in the considered bands. Similarly, a unique cloud mask was obtained by considering the union of all generated cloud masks.

4.2 Summary measurements

Once the cloud masks are available, summary statistics can be produced for each coverage. For example, Fig. 4 shows the histograms of the cloud percentage for all scenes of each coverage using a bin width of 5% cloud cover, the percentage being calculated on the basis of DROIs. The first histogram indicates the number of images and the second the percentage of total number of images for each bin. Figure 5 shows the union of all cloud masks obtained for coverages 1 and 2 respectively. For instance, in the latter case, it can be seen that more than 90% of the images of the reference coverage contain less than 5% of clouds. There is a total of 123 images whose calculated cloud coverage percentage exceeds 10% of their DROIs (not taking into account that clouds may fall in the sea only so that percentages may improve for some coastal scenes if only land were taken into account). Table 2 lists the identifiers of the 31 images of the reference coverage whose cloud cover is greater than 20% of their data ROI. The 4 scenes

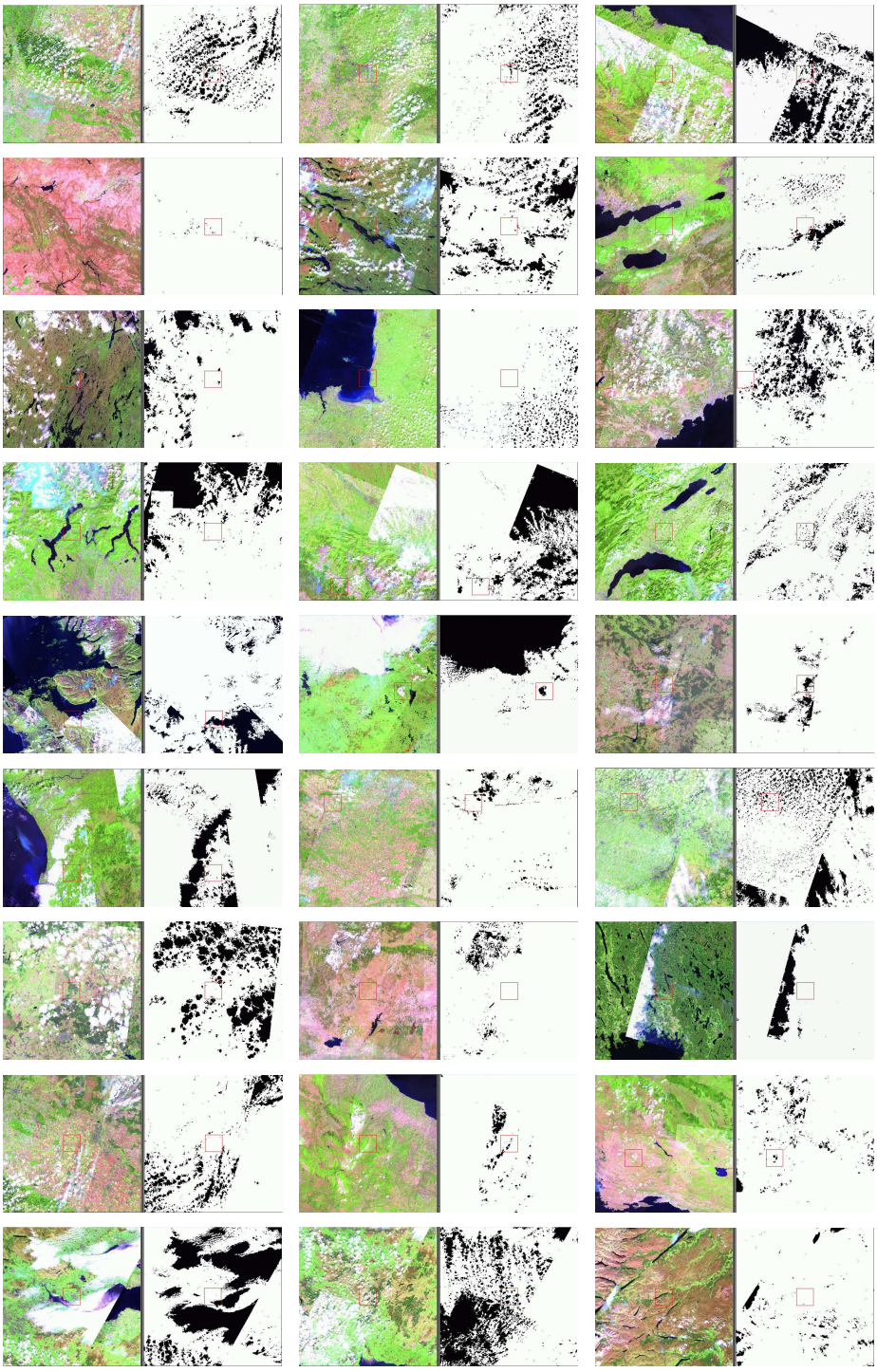

Figure 2: Gallery of satisfactory cloud masks.

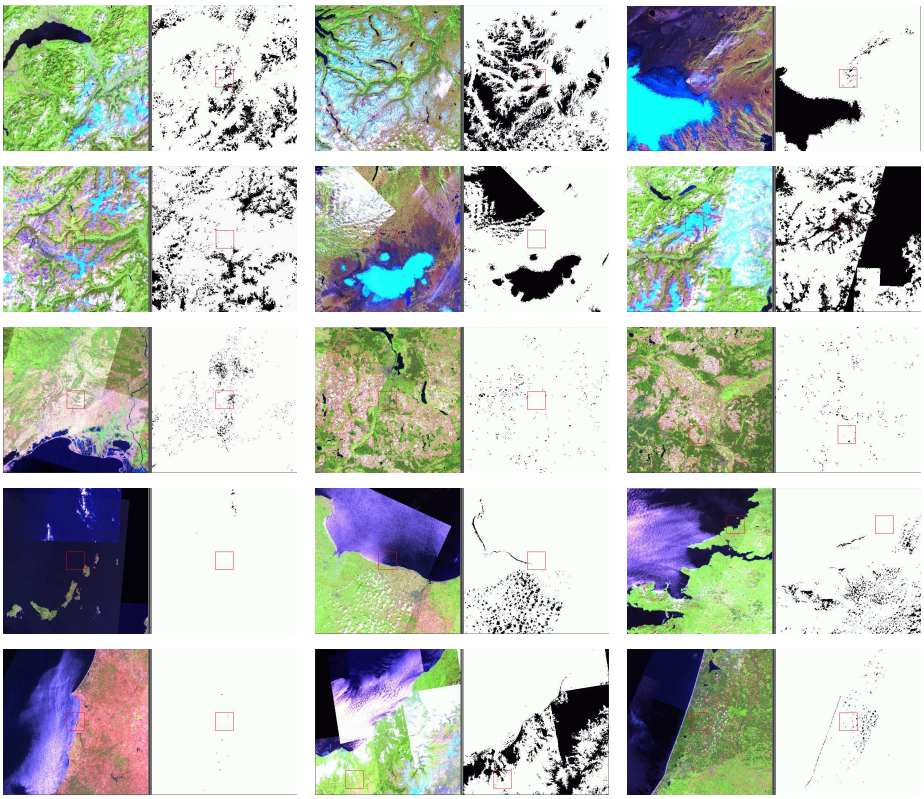

Figure 3: Gallery of unsatisfactory cloud masks (false positive errors and, to a lesser extent, false negative errors). Top two rows: ice and snow detected together with clouds. Third row: bright bare agricultural fields detected as clouds. Two bottom rows: undetected clouds over the sea (and beaches/breaking waves detected as clouds, last image).

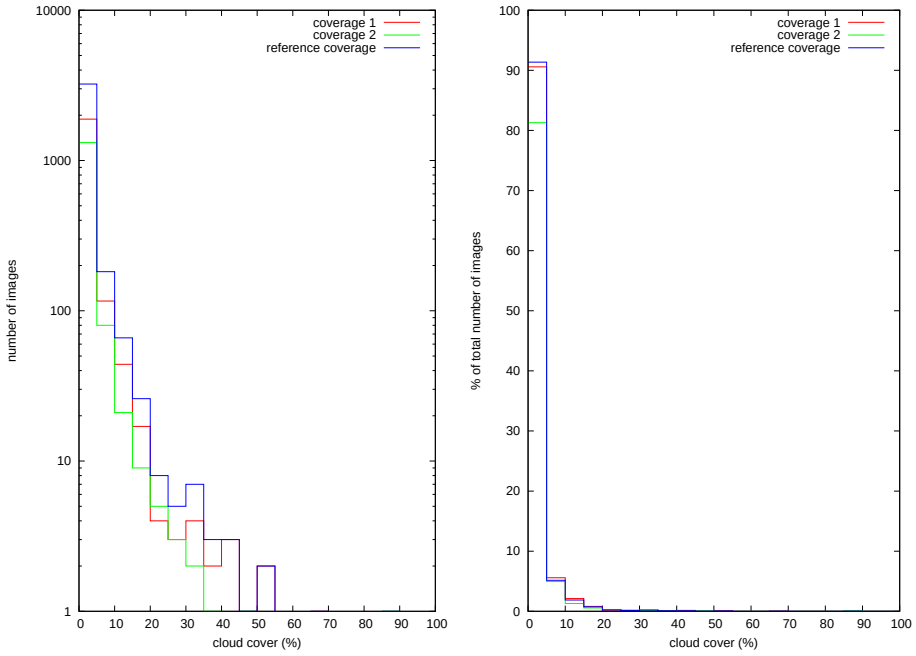

Figure 4: Frequency distribution of the cloud cover (in percentage of full data ROI) for all scenes of coverages 1 and 2 as well as the reference coverage. Left: in terms of number of images (logarithmic scale for y-axis). Right: normalised against the total number of images of each coverage. The histograms were produced using a bin width of 5% cloud cover.

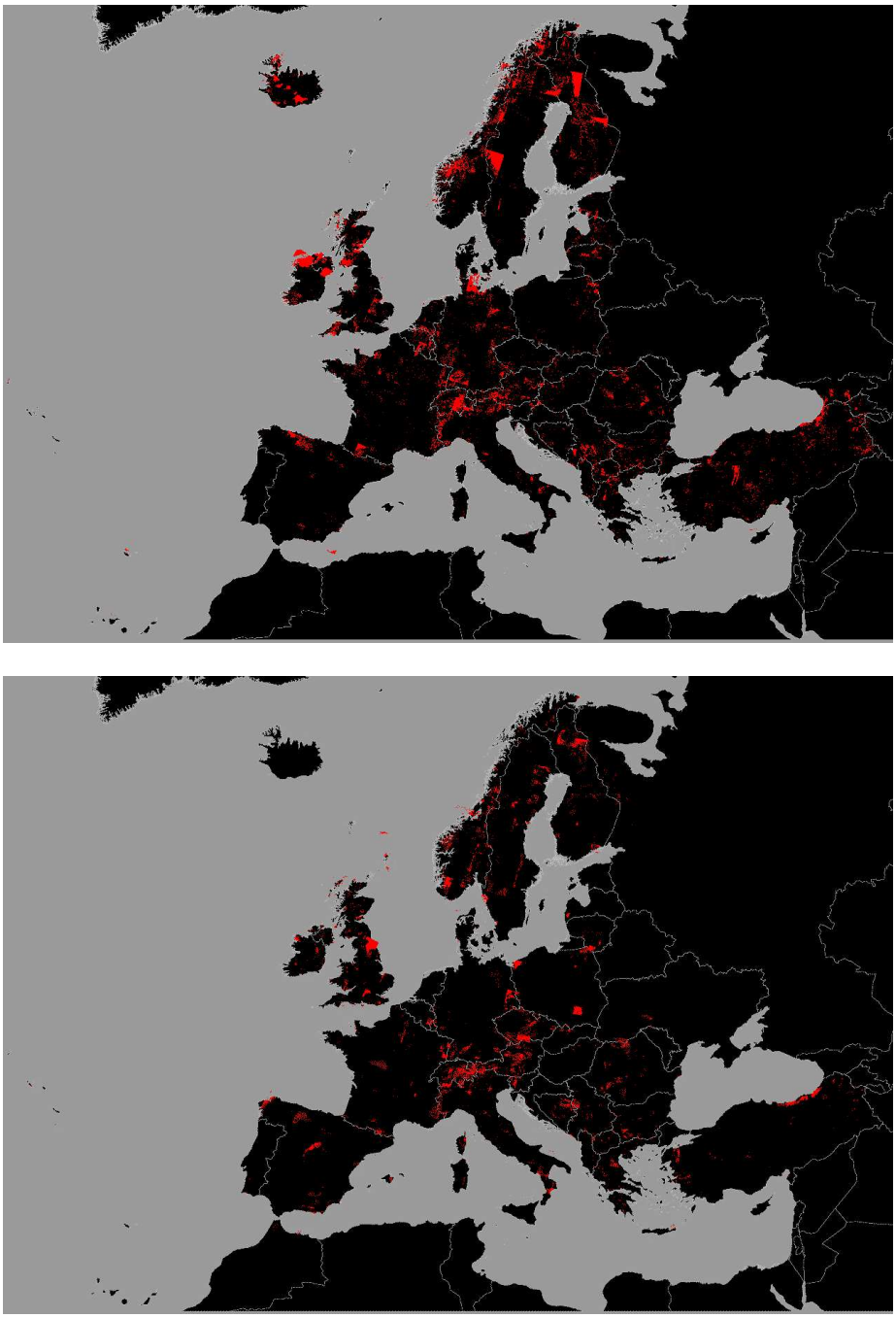

Figure 5: Cloud masks. Top: composition of the cloud masks of all 2,080 scenes of the first coverage. Bottom: composition of the cloud masks of all 1,619 scenes of the second coverage.

Table 2: Unique identifiers of the images of the reference coverage leading to a cloud cover greater than 20% of their data ROI (31 files out of a total of 3,533 files).

tile	date-time	sensor	centre	cloud (%)
43-B	20060426-1012	IL3	4635831544-CB	20
42-C	20060504-1033	SP4	4167128198-BC	20
43-A	20060916-1034	IL3	4370734847-DB	21
54-C	20060806-0944	IL3	5236446246-DA	22
33-C	20070529-1213	SP4	3060436246-DB	22
44-A	20061101-1050	SP4	4276940069-AA	22
44-A	20050630-1103	IL3	4247043769-BC	23
44-A	20070701-1103	SP5	4150943404-CC	24
44-D	20050702-1019	IL3	4908149296-AB	26
42-C	20060515-1022	SP4	4145927675-AB	27
44-D	20060502-1037	SP5	4771146249-AB	27
44-A	20070822-1134	SP4	4137742927-BA	28
62-B	20050730-0801	SP4	6867024961-DB	28
54-A	20060415-0954	SP4	5219142617-DB	30
25-B	20060909-1249	SP4	2917351133-CC	32
33-D	20070502-1125	IL3	3550335486-BA	32
33-C	20060817-1154	SP4	3217937133-AB	32
44-D	20070919-1022	SP5	4501346948-CA	32
44-D	20060809-1104	SP4	4538747441-CB	33
42-C	20060902-1028	IL3	4246726010-DC	34
33-C	20060908-1131	SP4	3443436337-AC	37
24-D	20070802-1300	SP4	2883549742-CB	37
42-C	20060610-1022	SP4	4133925259-BB	38
54-C	20060805-1005	IL3	5048649609-BB	43
42-C	20060610-1022	SP4	4222826061-AC	44
42-C	20060610-1022	SP4	4236326591-DB	44
42-C	20051230-1037	SP4	4244025564-BB	46
33-C	20050712-1156	IL3	3083036512-CB	51
44-A	20060715-1044	IL3	4469843797-AB	53
34-C	20060819-1253	SP4	3070748369-BB	69
53-A	20061230-0946	SP5	5092530859-DB	85

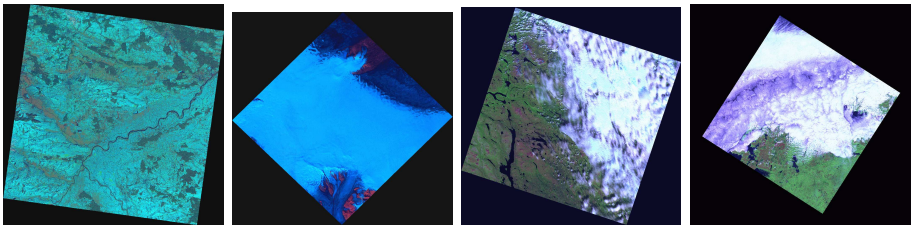

Figure 6: The 4 scenes with cloud masks deemed to be greater than 50% of their DROI. The names of these scenes are listed in the last four lines of table 2. They are displayed here in order of decreasing cloud cover. Note that the first scene is a 30th of December scene in the South-East of Poland with snow covered ground while the second scene shows part of the Vatnajökull glacier in Iceland.

Table 3: Clouds remaining within the territory of the participating countries when considering available imagery for each coverage in percentage of DROIs and CROIs.

	DROI			CROI		
	COV1	COV2	REF	COV1	COV2	REF
# Kpixels	25909	21660	10167	60322	44174	19836
Area (sqkm)	16193	13537	6354	37701	27608	12397
Area (%)	0.27	0.24	0.1	0.64	0.49	0.21

with cloud masks covering more than 50% of their full DROI are displayed in Fig. 6.

Fortunately, most cloudy areas are covered by more than one image so that most clouds will not appear in the produced mosaics. Indeed, when clouds are present in a region, the mosaicing algorithm automatically selects an image with no clouds if available. For instance, table 3 indicates the area of the regions that are always covered by clouds when considering all available imagery. For creating this table, measurements have been restricted to the territory of the participating countries. This table reveals that by substituting CROIs with DROIs, the permanent cloud cover is almost halved in all cases. For example, in the first coverage it would go from 0.64% to 0.27%. However, the quality of the orthorectification is only guaranteed within the country based ROIs. Permanent cloud area measurements performed at the country level are presented in table 4. Again, it can be observed that the use of DROIs rather than CROIs would often lead to a drastic decrease of the percentage of permanent cloud cover. Because snow and ice is usually detected as clouds (most common false positive error), all countries having large areas permanently covered with snow or ice show higher cloud percentage cover for all available imagery. This is the case Austria (AT), Switzerland (CH), Iceland (IS). Additional countries with remaining cloud cover larger than 1/1000 in the first coverage are Ireland (IE), Italy (IT), FYROM (MK), Malta (MT), Sweden (SE), Turkey (TR), and the United Kingdom (UK). The comprehensive table indicating permanent cloud cover statistics for all countries at least partly covered by the IMAGE-2006

Table 4: Clouds remaining within each participating countries when considering available imagery for each coverage in percentage of DROIs and CROIs. In this table, percentages are relative to the portion of the territory covered by available imagery rather than the whole territory).

	DROI			CROI		
	COV1	COV2	REF	COV1	COV2	REF
AL	0.03	0.13	0.00	0.21	1.02	0.07
AT	1.23	0.29	0.05	2.27	2.23	0.75
BA	0.00	0.08	0.00	0.43	1.06	0.01
BE	0.00	0.00	0.00	1.12	0.70	0.02
BG	0.03	0.48	0.00	0.28	0.75	0.00
CH	0.80	0.22	0.07	5.31	4.81	0.70
CS	0.04	0.03	0.00	0.70	0.17	0.00
CY	0.03	0.00	0.00	0.03	0.00	0.00
CZ	0.02	0.02	0.00	0.33	2.08	0.09
DE	0.06	0.02	0.00	0.29	0.28	0.00
DK	0.04	0.00	0.00	0.50	0.00	0.00
EE	0.04	0.02	0.00	0.04	0.02	0.00
ES	0.03	0.22	0.00	0.05	0.23	0.00
FI	0.03	0.30	0.00	0.20	0.31	0.02
FR	0.08	0.10	0.00	0.37	0.28	0.01
GR	0.03	0.30	0.00	0.36	0.44	0.00
HR	0.04	0.03	0.00	0.36	0.12	0.01
HU	0.01	0.00	0.00	0.76	0.02	0.00
IE	0.26	0.23	0.00	1.78	0.73	0.00
IS	4.92	-	4.92	4.92	-	4.92
IT	0.32	0.13	0.01	0.90	0.27	0.04
LI	0.00	0.00	0.00	0.46	0.15	0.15
LT	0.07	0.01	0.00	0.17	0.08	0.00
LU	0.00	0.00	0.00	1.20	2.38	0.73
LV	0.10	0.01	0.00	0.45	0.09	0.02
MK	0.11	0.00	0.00	1.24	0.66	0.14
MT	0.89	0.03	0.00	0.89	0.03	0.00
NL	0.00	0.03	0.00	0.46	0.07	0.00
NO	0.74	1.61	0.18	1.23	1.72	0.36
PL	0.04	0.01	0.00	0.17	0.47	0.01
PT	0.03	0.19	0.03	0.03	0.19	0.03
RO	0.06	0.21	0.02	0.08	0.40	0.02
SE	0.11	0.28	0.05	1.46	0.48	0.95
SI	0.01	0.11	0.00	2.30	3.43	0.32
SK	0.01	0.03	0.00	0.19	0.53	0.01
TR	0.32	0.18	0.02	0.33	0.25	0.02
UK	0.56	0.33	0.00	0.59	0.34	0.00

imagery is given in appendix A.

4.3 On cloud shadows

Beyond clouds, the occurrence of cloud shadows should be minimised in the produced mosaics. Rather than relying on complex spectral rules for detecting shadows, the generated masks are expanded on the fly during mosaicing so as to cover potential shadows. This expansion is achieved by performing a morphological dilation by a line segment [16, 15]. The length of the line segment is determined by the sun elevation angle and by assuming that clouds lie 2.5km above the ground. This assumption is valid for the most common type of clouds cluttering the IMAGE-2006 imagery, i.e., fair weather cumulus clouds (puffy cotton balls floating in the sky). Note that the directional dilation produces a continuous mask going from the detected cloud and reaching the estimated position of its shadow. This secures that the same image will be used to patch the cloud and its shadow. Consequently, the resulting mosaic has a higher spatial coherence than those authorising one to switch from one image to another when masking out a cloud and its shadow separately.

5 Conclusion

Although the algorithm described in this section was deemed sufficient for the purpose of creating cloud free mosaic, higher quality masks could probably be obtained using more elaborate algorithms in the future. Note that there exist very few publications detailing algorithms for cloud detection on SPOT and IRS imagery. Apart from basic procedures based on a unique intensity threshold level to identify the best cloud-free pixels among the pixels from the multiple images of the same region [9], most algorithms use very complex procedures based on neural networks [1, 7] so that they are not easily repeatable. Recently, a procedure based on Markov random fields was also put forward [8].

A simpler and potentially more effective method could exploit the availability of multiple imagery over the same areas to detect clouds thanks to change detection methods (for instance, clouds usually appear as well defined clusters in the bivariate histogram computed for the same bands within the overlapping region of a pair of images). Another promising approach could be based on the spectral rule based preliminary mapping procedures detailed in [2].

A Comprehensive cloud statistics

This appendix lists the percentage of the covered territory that is always covered by clouds. All countries at least partly covered by the IMAGE-2006 coverages are considered in this table. The percentage of each country that is indeed covered by the IMAGE-2006 imagery is given in a table in the appendix of [17]. Using the latter table, it can be seen, for example, that the Isle of Man (IM) is fully covered in terms of DROIs in the first coverage but almost not covered in the second coverage. However, from the table in the present appendix, it can be seen that the Isle of Man is cluttered by 10.43% of clouds in the first coverage. By contrast, it can be seen that the Vatican City State (VA) is fully covered in all coverages (even when considering CROIs) and is not contaminated by any cloud.

Table 5: Clouds remaining for all countries at least partly covered by the IMAGE-2006 data when considering available imagery for each coverage on the basis of DROIs and CROIs (the latter being restricted to buffered participating countries). In this table, percentages are relative to the portion of territory covered by imagery rather than the whole territory of the listed country. The ISO code of participating countries are typeset in bold (except for Serbia and Montenegro that are still appearing as the union of these two countries with the code CS).

	DROI			CROI		
	COV1	COV2	REF	COV1	COV2	REF
AD	0.00	2.08	0.00	0.00	2.16	0.00
AL	0.03	0.13	0.00	0.21	1.02	0.07
AM	5.96	1.46	4.97	5.96	1.46	4.97
AT	1.23	0.29	0.05	2.27	2.23	0.75
AZ	11.14	0.73	0.53	11.14	0.73	0.53
BA	0.00	0.08	0.00	0.43	1.06	0.01
BE	0.00	0.00	0.00	1.12	0.70	0.02
BG	0.03	0.48	0.00	0.28	0.75	0.00
BY	0.34	0.08	0.03	0.34	0.08	0.03
CH	0.80	0.22	0.07	5.31	4.81	0.70
CS	0.04	0.03	0.00	0.70	0.17	0.00
CY	0.03	0.00	0.00	0.03	0.00	0.00
CZ	0.02	0.02	0.00	0.33	2.08	0.09
DE	0.06	0.02	0.00	0.29	0.28	0.00
DK	0.04	0.00	0.00	0.50	0.00	0.00
EE	0.04	0.02	0.00	0.04	0.02	0.00
ES	0.03	0.22	0.00	0.05	0.23	0.00
FI	0.03	0.30	0.00	0.20	0.31	0.02
FR	0.08	0.10	0.00	0.37	0.28	0.01
GE	8.80	0.15	8.59	8.80	0.15	8.59
GG	0.00	-	0.00	0.00	-	0.00
GI	0.00	0.00	0.00	0.00	0.00	0.00

	DROI			CROI		
	COV1	COV2	REF	COV1	COV2	REF
GR	0.03	0.30	0.00	0.36	0.44	0.00
HR	0.04	0.03	0.00	0.36	0.12	0.01
HU	0.01	0.00	0.00	0.76	0.02	0.00
IE	0.26	0.23	0.00	1.78	0.73	0.00
IM	10.43	0.00	9.72	10.43	0.00	9.72
IQ	0.13	0.22	0.17	0.13	0.22	0.17
IR	2.22	0.90	0.81	2.22	0.90	0.81
IS	4.92	-	4.92	4.92	-	4.92
IT	0.32	0.13	0.01	0.90	0.27	0.04
JE	0.00	0.05	0.00	0.00	0.05	0.00
LI	0.00	0.00	0.00	0.46	0.15	0.15
LT	0.07	0.01	0.00	0.17	0.08	0.00
LU	0.00	0.00	0.00	1.20	2.38	0.73
LV	0.10	0.01	0.00	0.45	0.09	0.02
MA	0.03	4.37	3.48	0.03	4.37	3.48
MC	0.00	0.00	0.00	0.00	0.00	0.00
MD	0.03	0.28	0.02	0.03	0.28	0.02
MK	0.11	0.00	0.00	1.24	0.66	0.14
MT	0.89	0.03	0.00	0.89	0.03	0.00
NL	0.00	0.03	0.00	0.46	0.07	0.00
NO	0.74	1.61	0.18	1.23	1.72	0.36
PL	0.04	0.01	0.00	0.17	0.47	0.01
PT	0.03	0.19	0.03	0.03	0.19	0.03
RO	0.06	0.21	0.02	0.08	0.40	0.02
RU	0.05	1.14	0.34	0.05	1.14	0.34
SE	0.11	0.28	0.05	1.46	0.48	0.95
SI	0.01	0.11	0.00	2.30	3.43	0.32
SK	0.01	0.03	0.00	0.19	0.53	0.01
SM	0.00	0.60	0.00	0.00	0.60	0.00
SY	0.05	0.11	0.01	0.05	0.11	0.01
TR	0.32	0.18	0.02	0.33	0.25	0.02
UA	0.33	2.52	0.24	0.33	2.52	0.24
UK	0.56	0.33	0.00	0.59	0.34	0.00
VA	0.00	0.00	0.00	0.00	0.00	0.00

References

[1] Anonymous. Automatic cloud masking of SPOT imagery. *News from Prospace*, (44):42–47, May 1999.

[2] A. Baraldi, V. Puzzolo, P. Blonda, L. Bruzzone, and C. Tarantino. Automatic spectral rule-based preliminary mapping of calibrated Landsat TM and ETM+ images. *IEEE Transactions on Geoscience and Remote Sensing*, 44(9):2563–2586, September 2006. doi:10.1109/TGRS.2006.874140.

[3] H. Fliegel and T. Van Flandern. A machine algorithm for processing calendar dates. *Communications of the ACM*, 11(10):657, October 1968.

[4] D. Hall, G. Riggs, and V. Salomonson. Development of methods for mapping global snow cover using moderate resolution imaging spectroradiometer data. *Remote Sensing of Environment*, 54(2):127–140, November 95. doi:10.1016/0034-4257(95)00137-P.

[5] R. Irish. Landsat 7 automatic cloud cover assessment. In S. Shen and M. Descour, editors, *Proc. of Algorithms for Multispectral, Hyperspectral, and Ultraspectral Imagery VI*, volume 4049, pages 348–355. Society of Photo-Instrumentation Engineers, August 2000. doi:10.1117/12.410358.

[6] R. Irish, J. Barker, S. Goward, and T. Arvidson. Characterization of the Landsat-7 ETM+ automatic cloud cover assessment (ACCA) algorithm. *Photogrammetric Engineering and Remote Sensing*, 72(10):1179–1188, October 2006.

[7] J. Jang, A. Viau, F. Anctil, and E. Bartholomé. Neural network application for cloud detection in SPOT VEGETATION images. *International Journal of Remote Sensing*, 27(4):719–736, Feb 2006. doi:10.1080/01431160500106.

[8] S. Le Hégarat-Mascle and C. André. Reduced false alarm automatic detection of clouds and shadows on SPOT images using simultaneous estimation. In L. Bruzzone, editor, *Proceedings of Image and Signal Processing for Remote Sensing XIII*, volume SPIE-6748, page 674818, Firenze, 2007. doi:10.1117/12.737396.

[9] M. Li, S. Liew, L. Kwoh, and H. Lim. Improved cloud-free multi-scene mosaics of SPOT images. In *Proc. Asian Conf. Remote Sensing*, volume 1, pages 294–298, 1999.

[10] J. Meeus. *Astronomical Algorithms*. Willmann-Bell, Richmond, Virginia, 2nd edition, 1999.

[11] J. Richards and X. Jia. *Remote sensing digital image analysis*. Springer-Verlag, 3rd edition, 1999.

[12] P. Soille. *Morphological Image Analysis: Principles and Applications*. Springer-Verlag, Berlin Heidelberg New York, 2nd edition, 2003.

[13] P. Soille and C. Bielski. IMAGE-2006 Mosaic: Data ingestion and organisation. Technical report, European Commission, DG Joint Research Centre, 2008.

[15] P. Soille and H. Talbot. Directional morphological filtering. *IEEE Transactions on Pattern Analysis and Machine Intelligence*, 23(11):1313–1329, November 2001. doi:10.1109/34.969120. URL http://ams.jrc.it/soille/soille-talbot2001r.pdf.

[16] P. Soille, E. Breen, and R. Jones. Recursive implementation of erosions and dilations along discrete lines at arbitrary angles. *IEEE Transactions on Pattern Analysis and Machine Intelligence*, 18(5):562–567, May 1996. doi:10.1109/34.494646. URL http://www.computer.org/tpami/tp1996/i0562abs.htm.

[17] P. Soille, C. Bielski, and J. Nowak. IMAGE-2006 Mosaic: Analysis of image footprints —v.1.0—. Technical report, European Commission, DG Joint Research Centre, May 2008.

[18] Y. Zhang, B. Guindon, and J. Cihlar. An image transform to characterize and compensate for spatial variations of Landsat images. *Remote Sensing of Environment*, 82(2–3):173–187, October 2002. doi:10.1016/S0034-4257(02)00034-2.

European Commission

EUR 23636 EN – Joint Research Centre – Institute for Environment and Sustainability
Title: IMAGE-2006 Mosaic: SPOT-HRVIR and IRS-LISSIII Cloud Detection
Author: Pierre Soille
Luxembourg: Publications Office of the European Union
2011 – 19 pp. – 21.0 x 29.7 cm
EUR – Scientific and Technical Research series – ISSN 1831-9424 (online), 1018-5593 (print)
ISBN 978-92-79-20955-0
doi:10.2788/49355

Abstract
This report details the methodology adopted for detecting clouds from the IMAGE-2006 SPOT-4 HRVIR, SPOT-5 HRG, and IRS-LISS III imagery in view of creating mosaics. This detection is necessary for minimising cloud cover. Indeed, when clouds appear in a region where two or more images overlap, an image with no clouds in this region must be selected to cover this region. The availability of cloud masks enables an automatic selection during mosaicing. The proposed methodology is based on a modified cloud detection algorithm originally developed for Landsat sensors. The modifications address the lack of a thermal channel for the IMAGE-2006 imagery. Spatial context is also exploited in a second stage thanks to a series of morphological transformations. Overall, the produced cloud masks are satisfactory for automatically minimising cloud cover during mosaicing.

The mission of the JRC is to provide customer-driven scientific and technical support for the conception, development, implementation and monitoring of EU policies. As a service of the European Commission, the JRC functions as a reference centre of science and technology for the Union. Close to the policy-making process, it serves the common interest of the Member States, while being independent of special interests, whether private or national.

JRC
EUROPEAN COMMISSION

LB-NA-23636-EN-N

Publications Office